Journal of Experimental Pharmacology

Dovepress
open access to scientific and medical research

Open Access Full Text Article

ORIGINAL RESEARCH

Identifying Potential Human Monoacylglycerol Lipase Inhibitors from the Phytoconstituents of *Morinda Citrifolia* L. Fruits by in silico Pharmacology and in vitro Study

Asman Sadino[1,2,*], Nyi Mekar Saptarini[3], Jutti Levita[4,*], Dwi Syah Fitra Ramadhan[5], Adryan Fristiohady[6], Supat Jiranusornkul[7]

[1]Doctoral Program in Pharmacy, Faculty of Pharmacy, Universitas Padjadjaran, Sumedang, West Java, 45363, Indonesia; [2]Department of Pharmacology and Clinical Pharmacy, Faculty of Mathematics and Natural Sciences, Garut University, Garut, West Java, 44151, Indonesia; [3]Department of Pharmaceutical Analysis and Medicinal Chemistry, Faculty of Pharmacy, Universitas Padjadjaran, Sumedang, West Java, 45363, Indonesia; [4]Department of Pharmacology and Clinical Pharmacy, Faculty of Pharmacy, Universitas Padjadjaran, Sumedang, West Java, 45363, West Java, Indonesia; [5]Department of Pharmacy, Poltekkes Kemenkes Makassar, Makassar, South Sulawesi, 90222, Indonesia; [6]Faculty of Pharmacy, Halu Oleo University, Kendari, Southeast Sulawesi, 93132, Indonesia; [7]Department of Pharmaceutical Science, Faculty of Pharmacy, Chiang Mai University, Chiang Mai, Thailand

*These authors contributed equally to this work

Correspondence: Jutti Levita, Department of Pharmacology and Clinical Pharmacy, Faculty of Pharmacy, Universitas Padjadjaran, Sumedang, West Java, 46363, Indonesia, Email jutti.levita@unpad.ac.id

Background: Human monoacylglycerol lipase (MGL) is accountable for the hydrolysis of 2-arachidonoylglycerol (2-AG), thus contributing pivotally to neuroprotection because 2-AG is the main source of arachidonic acid, the precursor of prostaglandins production. Inhibiting MGL reduces inflammatory damage in the ischemic brain and enhances cerebral blood flow. Plants have been reported for their neuroprotective effect, such as *Morinda citrifolia* on pentylenetetrazol (PTZ)-induced kindling seizures in mice, by reducing the seizures and restoring behavioral and biochemical changes, although the mechanism is not described.

Purpose: To evaluate the binding affinity and stability of phytoconstituents in *M. citrifolia* fruits toward human MGL (PDB ID 3PE6), compared to the known MGL inhibitors (JZL195 and ZYH). The in silico pharmacology study was validated by an in vitro study of the phytosterols and the ethanol extract of *M. citrifolia* fruits (EEMC) towards MGL.

Methods: Initially, nine phytoconstituents of *M. citrifolia* fruits were docked to the catalytic pocket of human MGL (PDB ID: 3PE6), and compounds with the best affinity were subjected to a molecular dynamic (MD) simulation. The in vitro study was performed using the MGL inhibitor screening assay kit.

Results: The best binding affinity and stability toward human MGL were shown by stigmasterol and beta-sitosterol, and the MM-PBSA total binding energy of stigmasterol and beta-sitosterol to MGL is stronger than that of JZL195 and ZYH. Moreover, beta-sitosterol and EEMC inhibit MGL with an IC_{50} value of, respectively, 8.10 µg/mL and 196.20 µg/mL, while JZL195 shows an IC_{50} of 0.028 µg/mL.

Conclusion: Beta-sitosterol of *Morinda citrifolia* fruits may have the potential to protect human neurons by occupying the catalytic site of human MGL, thus competitively inhibiting the substrate of the enzyme. However, the inhibitory activity towards human MGL is lower than JZL195.

Keywords: 2-arachidonoylglycerol, beta-sitosterol, phytosterols, prostaglandin, serine hydrolase, stigmasterol

Introduction

Monoacylglycerol lipase (MGL), a serine hydrolase enzyme, works by hydrolyzing the endocannabinoid 2-arachidonoylglycerol (2-AG) to produce fatty acids and glycerol.[1] MGL is distributed in discrete brain areas, eg, the hippocampus, the cerebellum, the anterodorsal nucleus of the thalamus, and the cortex.[2] A characterization study described that

Received: 12 May 2024
Accepted: 19 September 2024
Published: 23 September 2024

both rat MGL and mouse MGL showed 84.2% and 83.8%, respectively, of sequence identity with human MGL, with its highly conserved catalytic triad, consisting of residues Ser122, Asp239, and His269.[3] Furthermore, this enzyme was described to contain one sulfhydryl-sensitive site essential for its activity and two cysteine residues, Cys208 and Cys242, in the catalytic site, and a covalent interaction with these two residues is required for inhibiting the enzyme activity.[3,4] Interestingly, a 3D QSAR pharmacophore study by Afzal and co-workers described the requirements of three features for MGL inhibitors. These pharmacophore features comprise one hydrogen bond acceptor (HBA), one positive center, and three aromatic rings (to occupy the hydrophobic space and bind with the hydrophobic amino acids).[5] In another study, the pharmacophore of MGL inhibitors should consist of four HBAs, one aromatic, and three optional hydrophobic features.[6]

Many studies have delineated that MGL contributes crucially to numerous physiological and pathological pathways, such as neuroprotection and inflammation,[1] because 2-AG, the substrate of MGL, is the main source of arachidonic acid (AA), the precursor in the biosynthesis of prostaglandins and leukotrienes.[7] The dual functions of MGL are described as controlling the levels of 2-AG thus exhibiting neuroprotective effects,[8–10] and directly targeting microglia.[11] Considering that MGL is the main enzyme involved in AA synthesis in the brain, the inhibition of this enzyme may have the potential to cure neurodegenerative and neuropsychiatric diseases, chronic pain, or cancer.[10]

Plants have the potential to be developed as neuroprotective agents by altering various pathways as reported in many previous studies.[12–16] Plant terpenoids (pristimerin and euphol) were reported to reversibly reduce MGL activity by targeting Cys201 and Cys208.[17] A recent study by Ali and coworkers reported the neuroprotective effect of *M. citrifolia* fruit extract given orally towards pentylenetetrazol (PTZ)-induced kindling seizures in mice by reducing the seizures and restoring behavioral and biochemical changes.[16]

Considering the potential of *M. citrifolia* fruit as a neuroprotective drug, this study aims to evaluate the binding affinity and stability of phytoconstituents in *M. citrifolia* fruits toward human MGL, compared to the known MGL inhibitors (JZL195 and ZYH) by the in silico pharmacology study, and further validated by the in vitro study.

Materials and Methods

Hardware and Software

The hardware is a computer with an Intel (R) Core i5-8500 CPU @ 4.30GHz (6CPUs) processor, 4096 MB RAM, 2TB hard drive, 120GB solid-state drive, and Intel HD Graphics NVIDIA GeForce GTX 1080 Ti.

The computer is equipped with Windows 7 and Linux Ubuntu 16.04 operating systems equipped with Gaussian 09, Gauss View 5.0.8, AutoDock 4.2 equipped with MGLTools 1.5.6 was downloaded from The Scripps Research Institute official website (http://autodock.scripps.edu/), BIOVIA Discovery Studio Visualizer 2016 (https://discover.3ds.com/discovery-studio-visualizer-download), GROMACS 2016.3 (https://manual.gromacs.org/2016.3/index.html), ACPYPE (AnteChamber PYthon Parser interface), ForceGen 0.4, VMD 1.9.2, and MMPBSA.py.

Ligand Preparation and Pre-ADMET Prediction

The 3D structure of stigmasterol (PubChem CID 5280794; molecular formula: $C_{29}H_{48}O$; molecular weight: 412.7g/mol), beta-sitosterol (PubChem CID 222284; molecular formula: $C_{29}H_{50}O$; molecular weight: 414.7 g/mol), quercetin (PubChem CID 5280343; molecular formula: $C_{15}H_{10}O_7$; molecular weight: 302.23 g/mol), damnacanthal (PubChem CID 2948; molecular formula: $C_{16}H_{10}O_5$; molecular weight: 282.25 g/mol), asperuloside (PubChem CID 84298; molecular formula: $C_{18}H_{22}O_{11}$; molecular weight: 414.4 g/mol), americanin (PubChem CID 131751085; molecular formula: $C_{18}H_{16}O_6$; molecular weight: 328.3 g/mol), ursolic acid (PubChem CID 64945; molecular formula: $C_{30}H_{48}O_3$; molecular weight: 456.7 g/mol), rutin (PubChem CID 5280805; molecular formula: $C_{27}H_{30}O_{16}$; molecular weight: 610.5 g/mol), and scopoletin (PubChem CID 5280460; molecular formula: $C_{10}H_8O_4$; molecular weight: 192.17 g/mol) was obtained from the PubChem Compound databases. The geometry energy of the ligands was optimized by MMFF94, which is intended to produce accurate geometric structures.[18]

The ligands were predicted for their absorption and distribution in the blood-brain barrier and their toxicity-mutagenicity properties in mice and rats using the online Pre-ADMET software (https://preadmet.webservice.bmdrc.org/).

Macromolecule Preparation

The X-ray structure of human monoacylglycerol lipase (MGL) (PDB ID: 3PE6, resolution 1.35 Å, PDB DOI https://doi.org/10.2210/pdb3PE6/pdb, deposited by Schubert and Schalk-Hih in 2010 and released in 2011) in complex with its inhibitor ZYH (2-cyclohexyl-1,3-benzoxazol-6-yl)-[3-(4-pyrimidin-2-ylpiperazin-1-yl)azetidin-1-yl]methanone, was downloaded from Protein Data Bank. The macromolecules were prepared by removing the water molecules and their unique ligand and adding polar hydrogen and a Kollman charge.[19] All procedures were conducted using AutoDock 4.2.

Molecular Docking Simulation

This step was performed using AutoDock 4.2,[19–22] by docking the nine phytoconstituents and the two standard inhibitors as the ligands in the active site of human MGL (PDB ID: 3PE6). To validate the molecular docking protocol, a re-docking analysis of the co-crystallized ligand (ZYH) with 3PE6 was performed. The RMSD between the experimental and predicted poses of ZYH was determined. The binding affinity in terms of the docking score (kcal/mol), the inhibitory constant (Ki in μM), the hydrogen bond and the hydrophobic interactions, and the close contact residues were recorded and compared.[19–22]

Molecular Dynamics Simulation

The molecular dynamics (MD) simulation was carried out using the GROMACS (Groningen Machine for Chemical Simulation) 2016.3 software with the AMBER99SB-ILDN force field as described elsewhere. The topology and ligand parameters were generated and the particle mesh Ewald method was used to calculate the electrostatic force. The system was neutralized using the NaCl model and the solvation process was carried out with the TIP3P water cube model.[19,23–31] In this study, MD simulation was performed up to 250 ns with a 2-frame timestep and the root mean square deviation (RMSD), root mean square fluctuation (RMSF), and radius of gyration (Rg) were calculated, followed by a post-MD simulation analysis of the molecular mechanics-Poisson-Boltzmann surface area (MM-PBSA) binding free energy.

MD evaluates the conformational stability of the complex between ligand and protein and the binding affinity of the ligand,[24] by calculating the RMSD and RMSF values.[25] RMSD measures the deviation of a protein's backbone from its initial conformation to its final conformation. A stable protein will show minimal deviation in its backbone. RMSF is used to identify the flexible regions of the protein-ligand complexes. Less-organized proteins will have higher RMSF fluctuations.[24] MD simulation comprises five sequential steps, energy minimization, NVT (simulation based on constant number, constant volume, and constant temperature) heating, NPT (simulation based on constant number, constant pressure, and constant temperature) equilibration, NPT pre-production simulation, and production simulation.[26,27] The topology and coordinate file for the amino acid residues were built by employing the force field ff19SB, while those of the ligands were generated using the General Amber Force Field (GAFF). The missing force field parameters of the ligands were restored by the Parmchk2 tool. The electrostatic force was computed using Particle Mesh Ewald Molecular Dynamics.[28,29] The system neutralization was carried out by adding sodium and chloride ions and the solvation was corrected using the TIP3P (a 3-site rigid water molecule with charges and Lennard-Jones parameters assigned to each of the 3 atoms) water cube model. The preparation steps included minimization, heating to 310 °K, and equilibration of temperature and pressure.[30,31]

Trajectory Analysis and Visualization (MM-PBSA Binding Free Energy Calculations)

The molecular mechanics' energies combined with the Poisson-Boltzmann surface area and surface area continuum solvation (MM-PBSA) is an efficient and reliable free energy simulation method to model molecular recognition and to calculate the binding free energy of non-covalently bound complexes,[32] using the g_mmpbsa package embedded in the GROMACS (https://www.gromacs.org/), with the binding free energy of complex (ΔGbind) is described as follows:

$$\Delta G_{bind} = G_{complex} - G_{rec} - G_{ligand}$$

$$\Delta G_{bind} = \Delta EMM + \Delta G_{sol} - T\Delta S$$

$$\Delta EMM = \Delta E_{bond} + \Delta E_{angle} + \Delta E_{torsion} + \Delta E_{vdW} + \Delta E_{ELE}$$

$$\Delta G_{sol} = \Delta G_{PB} + \Delta G_{SA}$$

The dielectric constant of the solvent was set at 80 (water).[33] The nonpolar contribution was calculated as the water-accessible surface area at a radius of 1.4 Å. The protein-ligand binding free energy was calculated based on the output of MD simulation on 1000 snapshots taken from 250 ns simulation trajectories. The resulting MD trajectories of the ligand-protein complexes were processed through the CPPTRAJ tool.[34]

Plant Materials and Preparation of the Extract

The fresh ripe fruits were harvested in August 2023 (outside temperature, 25 to 30°C) at the plantation DK Manggen, Nogosari District, Boyolali Regency (Google coordinates: 7°26'38.1"S 110°46'07.5"E), Central Java, Indonesia. The fruit samples were taxonomically identified by Arifin Surya Dwipa Irsyam (https://www.scopus.com/authid/detail.uri?authorId=57211286941; https://herbarium.sith.itb.ac.id/profil-kurator/), the certified botanist at the School of Life Sciences and Technology, Bandung Institute of Technology (Bandung, West Java, Indonesia), and were confirmed as *Morinda citrifolia* L. (specimen no. 5745/2023). The plant specimens matched the characteristics described in flowering plant taxonomic references.[35–37]

The fruits were washed under tap water to separate any soil, dust, and other foreign inorganic matter, and then cleaned according to standard pharmacognosy laboratory procedures, such as medicinal plant materials being completely free of visible signs of mold or insect contamination, as well as other animal contamination, including animal excretes. Fruits with abnormal odors, discoloration, slime, or deterioration signs were removed.[38] The clean fruits were cut and dried in an oven at 40 °C. The dried samples were mashed using a pestle in a white porcelain mortar for extraction.

Dried *M. citrifolia* coarse powder fruit (1500 g) was macerated with a total of 20 L of 96% ethanol for 3×24 h (approximately 6.66 L/24 h to completely soak the coarse powder fruit) to obtain 379.4 g extract (yield, 25.29% w/w). The extract was thickened using a vacuum rotary evaporator (Buchi) at 60°C and 65 rpm.

Effects of EEMC on Human Monoacylglycerol Lipase by in vitro Study

A commercially available Monoacylglycerol Lipase Inhibitor Screening Assay Kit (Item No. 705192, Cayman Chemical Company; https://www.caymanchem.com/product/705192/monoacylglycerol-lipase-inhibitor-screening-assay-kit) was used. The principle of the reaction is that human MGL hydrolyzes 4-nitrophenyl acetate, the artificial substrate in the kit, to produce a yellow compound, namely 4-nitrophenol, which is measured at 405–412 nm.[39] The kit contains several reagents, such as the MGL assay buffer (item No. 705195), MGL substrate (item No. 705193), a solution of human recombinant MGL (item No. 705194), JZL195 inhibitor assay reagent (item No. 700307) as the positive control, a 96-well plate (item No. 400014), and a 96-well cover sheet (item No. 400012) (https://cdn.caymanchem.com/cdn/insert/705192.pdf). The reagent preparation and the in vitro study were carried out by strictly following the protocol instructions. The inhibitors tested were increased concentrations of EEMC (0.1; 1.0; 10; 100; and 1000 µg/mL) and beta-sitosterol (0.05; 0.1; 0.5; 1.0; and 10 µg/mL). After mixing the contents of the wells and incubating for 15 min at room temperature, the reactions were initiated by adding 10 µL of MGL substrate to all the wells, and the mixture was incubated at 37 °C for 10 minutes and measured at 405 nm. The MGL inhibitory activity was calculated using the following equation:

$$\%\ \text{activity} = \frac{\text{corrected inhibitor activity}}{\text{corrected 100\% initial activity}} \times 100$$

The concentration of sample required to inhibit 50% of monoacylglycerol lipase activity under the above conditions was defined as the IC_{50} value. The monoacylglycerol lipase inhibitory activity of the samples was calculated, and its IC_{50} values were determined using GraphPad Prism software.

Table 1 Pre-ADMET Prediction (https://preadmet.webservice.bmdrc.org/) of Absorption-Distribution in Blood-Brain Barrier and Toxicity-Mutagenicity of Nine Phytoconstituents in Morinda Citrifolia Fruits

Name of the Compound	Prediction of Absorption in Caco-2 Cells for Oral Administration Drugs (nm sec)	Prediction of Distribution in Blood-Brain Barrier (%)	Toxicity (Ames Test)	Mutagenicity	
				In Mice	In Rats
Americanin	17.78	0.22	Mutagen	**Negative**	**Negative**
Asperuloside	12.95	0.02	Mutagen	Positive	**Negative**
Beta-sitosterol	**52.37**	**19.89**	**Non-mutagen**	Positive	**Negative**
Damnacantal	14.25	0.95	Mutagen	**Negative**	Positive
Quercetin	3.41	0.17	Mutagen	**Negative**	Positive
Rutin	7.91	0.03	**Non-mutagen**	**Negative**	**Negative**
Scopoletin	0.28	0.64	Mutagen	**Negative**	Positive
Stigmasterol	**52.34**	**19.89**	**Non-mutagen**	Positive	**Negative**
Ursolic Acid	21.86	**8.01**	**Non-mutagen**	Positive	Positive

Notes: A Caco-2 absorption value of > 70 indicates high permeability; a Caco-2 absorption value of 4–70 indicates medium permeability; a Caco-2 absorption value of < 4 indicates low permeability.
A % BBB value of < 0.1 indicates low penetration; a % BBB value of 0.1–2.0 indicates medium penetration; a % BBB value of > 2.0 indicates high penetration.
Bold indicates good results.

Statistical Analysis

Data were analyzed using GraphPad Windows v.6.07 software (https://www.graphpad.com/support/prism-6-updates/).

Results

The Pre-ADMET Properties, Binding Mode, and Affinity of the Ligands Towards MGL

The pre-ADMET properties are tabulated in Table 1, showing that beta-sitosterol and stigmasterol have the potential to be absorbed in the intestine cells with medium permeability, distributed in the blood-brain barrier with high penetration property, non-mutagenic, and non-carcinogenic.

To validate the method, molecular docking was initiated by re-docking ZYH (the inhibitor co-crystallized in the protein) to the binding pocket of MGL (3PE6). Figure 1 shows a satisfactory RMSD value of 0.921 Å (RMSD less than 2.0 Å), indicating that both ZYH molecules occupied the catalytic pocket of the enzyme in almost the same geometrical structure and conformation, thus confirming the validity of the molecular docking method. The binding energy of the docked-ZYH is −12.94 kcal/mol.

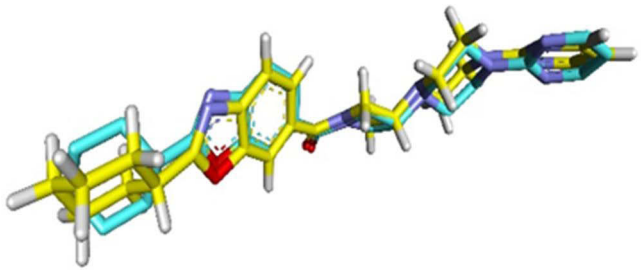

Figure 1 The superimposition of two molecules of ZYH (the yellow color molecule represents the docked- ZYH; the cyan color molecule represents the co-crystallized ZYH) in the catalytic pocket of MGL. The obtained consecutive RMSD value is 0.921 Å.

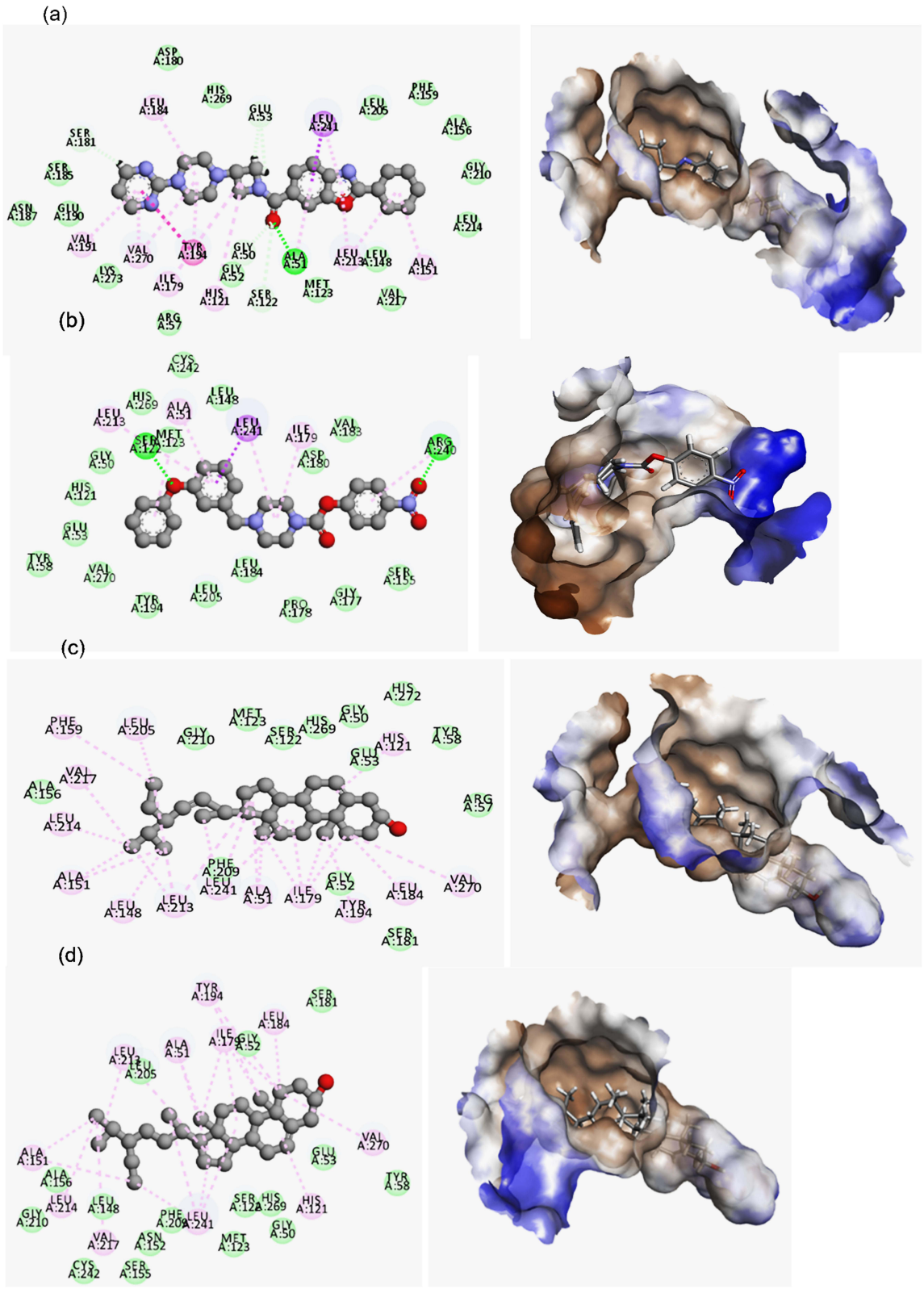

Figure 2 The binding mode of (**a**) ZYH; (**b**) JZL195; (**c**) stigmasterol; and (**d**) beta-sitosterol with human MGL. Figures on the left depict the amino acid residues involved in the interaction. Figures on the right illustrate the position of the ligands in the catalytic pocket of human MGL. Green dashed lines represent conventional hydrogen bonds; pink dashed lines represent pi interaction; green circles represent Van der Waals interaction.

The molecular docking simulation reveals that ZYH could enter the catalytic site of MGL and build hydrophobic interaction (Figure 2a) as follows: the Van der Waals interaction with 20 amino acids including Gly50, Gly52, Glu53, Arg57, **Ser122** (one of the catalytic triad residues) (Zvonok et al, 2008a), Met123, Leu148, Ala156, Phe159, Asp180, Ser181, Ser185, Asn187, Glu190, Leu205, Gly210, Leu214, Val217, **His269** (one of the catalytic triad residues) (Zvonok et al, 2008a), and Lys273, and other hydrophobic interactions, such as with Leu241 (one pi-sigma, one pi-alkyl), Tyr194 (one pi-pi stacking, two pi-alkyl interaction), Leu184 (one pi-alkyl), Val191 (one pi-alkyl), Val270 (two pi-alkyl interactions), Ile179 (one pi-alkyl interaction), His121 (one pi-alkyl), Leu213 (two pi-alkyl interactions), and Ala151 (one pi-alkyl), and only one hydrogen bond with Ala51.

Interestingly, the nine bioactive compounds found in *M. citrifolia* fruit (tabulated in Table 2), including sterols (stigmasterol and beta-sitosterol), lignans (americanin), iridoid glycoside (asperuloside), anthraquinones (damnacanthal), flavonoids (quercetin and rutin), coumarin (scopoletin), and triterpenoids (ursolic acid), also show interaction with important residues in the catalytic site of human MGL with the binding energy, in order from the highest to the lowest, is scopoletin (−6.14 kcal/mol), rutin (−7.18 kcal/mol), asperuloside (−7.20 kcal/mol), damnacanthal (−7.60 kcal/mol),

Table 2 The Binding Affinity of Nine Phytoconstituents in Morinda Citrifolia Fruits to Human Monoacylglycerol Lipase Compared with the Inhibitors

Name of the Ligand or Plant Metabolite	Group of Metabolites	Description in PubChem	Binding Affinity in Terms of Docking Score (kcal/mol)
Quercetin	Flavonoids	PubChem CID 5280343; molecular formula: $C_{15}H_{10}O_7$; molecular weight: 302.23 g/mol	−7.88
Damnacanthal	Anthraquinones	PubChem CID 2948; molecular formula: $C_{16}H_{10}O_5$; molecular weight: 282.25 g/mol	−7.60
Asperuloside	Iridoid glycoside	PubChem CID 84298; molecular formula: $C_{18}H_{22}O_{11}$; molecular weight: 414.4 g/mol	−7.20
Americanin	Lignans	PubChem CID 131751085; molecular formula: $C_{18}H_{16}O_6$; molecular weight: 328.3 g/mol	−7.84
Ursolic acid	Triterpenoids	PubChem CID 64945; molecular formula: $C_{30}H_{48}O_3$; molecular weight: 456.7 g/mol	−8.82
Rutin	Flavonoids	PubChem CID 5280805; molecular formula: $C_{27}H_{30}O_{16}$; molecular weight: 610.5 g/mol	−7.18
Stigmasterol	Steroids	PubChem CID 5280794; molecular formula: $C_{29}H_{48}O$; molecular weight: 412.7g/ mol	−11.50
Beta-Sitosterol	Steroids	PubChem CID 222284; molecular formula: $C_{29}H_{50}O$; molecular weight: 414.7 g/mol	−11.20
Scopoletin	Coumarin	PubChem CID 5280460; molecular formula: $C_{10}H_8O_4$; molecular weight: 192.17 g/mol	−6.14
JZL195 (MGL inhibitor)	4-nitrophenyl 4-(3-phenoxy benzyl) piperazine -1-carboxylate	N/A in PubChem	−9.65
ZYH (MGL inhibitor)	(2-cyclohexyl-1,3-benzoxazol-6-yl)-[3-(4-pyrimidin-2-ylpiperazine-1-yl) azetidine -1-yl]methanone	N/A in PubChem	−12.94

americanin (−7.84 kcal/mol), quercetin (−7.88 kcal/mol), ursolic acid (−8.82 kcal/mol), beta-sitosterol (−11.20 kcal/mol), and stigmasterol (−11.50 kcal/mol), thus revealing the best affinity of both stigmasterol and beta-sitosterol to human MGL.

It is visualized that stigmasterol (Figure 2b) binds to the catalytic site of MGL by building hydrophobic or Van der Waals interaction with 11 amino acids including Gly50, Gly52, Arg57, Tyr58, **Ser122** (one of the catalytic triad residues),[40] Met123, Ala156, Phe209, Gly210, **His269** (one of the catalytic triad residues),[40] and His272, and other hydrophobic interactions with Leu205 (one pi-alkyl), Phe159 (one pi-alkyl), Val217 (one pi-alkyl), Leu214 (one pi-alkyl) , Ala151 (two pi-alkyl), Leu148 (one pi-alkyl), Leu213 (three pi-alkyls), Leu241(three pi-alkyls), Ala51 (two pi-alkyls), Ile179 (four pi-alkyls), Tyr194 (one pi-alkyl), Leu18 (one pi-alkyl), Val270 (one pi-alkyl), and His121 (one pi-alkyl).

Similarly, beta-sitosterol (Figure 2c) also occupies the hydrophobic catalytic site of human MGL by building hydrophobic or Van der Waals interaction with Gly50, Gly52, Glu53, Tyr58, **Ser122** (one of the catalytic triad residues),[40] Met123, Leu148, Asn152, Ser155, Ala156, Ser181, Leu205, Gly210, Phe209, **Cys242** (one of the important residues required to inhibit MGL activity),[4,40] **His269** (one of the catalytic triad residues),[3] and other hydrophobic interactions with Leu184 (one pi-alkyl), Tyr194 (two pi-alkyls), Ile179 (four pi-alkyls), Ala51 (one pi-alkyl), Leu213 (two pi-alkyls), Ala151 (two pi-alkyls), Leu214 (one pi-alkyl), Val217 (one pi-alkyl), Leu241 (four pi-alkyls), His121 (one pi-alkyl), and Val270 (one pi-alkyl).

Furthermore, we analyzed the molecular docking simulation of JZL195 (Figure 2d), a standard human MGL inhibitor, generally employed in the in vitro study. JZL195 interacts with the enzyme by building conventional hydrogen bonds with 2 amino acids, namely, Ser122 (one of the catalytic triad residues),[3] and Arg240, which confirms that this inhibitor could occupy the catalytic site of the enzyme. JZL195 builds Van der Waals interaction with 17 amino acids including Gly50, Glu53, Tyr58, His121, Met123, Leu148, Ser155, Gly177, Pro178, Asp180, Val183, Leu184, Tyr194, Leu205, **Cys242** (one of the important residues required to inhibit MGL activity),[3,4] **His269** (one of the catalytic triad residues),[40] and Val270, and other hydrophobic interactions with Leu241 (one pi-sigma, one pi-alkyl), Ile179 (one pi-alkyl), Ala51 (one pi-alkyl), and Leu213 (one pi-alkyl). The interactions of JZL195 towards MGL resemble the interactions of beta-

Table 3 The Inhibitory Constant (Ki) and Residues Involved in the Interaction of Nine Phytoconstituents in M. Citrifolia Fruit to Human Monoacylglycerol Lipase Compared with the Inhibitors

Ligands	Ki (μM)	Type of Interaction		
		Hydrogen Bond	Van der Waals	Pi Interaction
Stigmasterol	0.0037	Ala51	Ala156, Gly50, Gly52, Arg57, Tyr58, **Ser122**, Met123, Phe209, Gly210, **His269**, His272	Leu205, Phe159, Val217, Leu214, Ala151, Leu148, Leu213, Leu241, Ala51, Ile179, Tyr194, Leu18, Val270, His121
Beta-sitosterol	0.0061	Ala51	Ser181, Gly50, Gly52, Glu53, Tyr58, **Ser122**, Met123, Leu148, Asn152, Ser155, Ala156, Leu205, Phe209, Gly210, ***Cys242*, His269**	Leu184, Tyr194, Ile179, Ala51, Leu213, Ala151, Leu214, Val217, Leu241, His121, Val270
JZL195 (MGL inhibitor)	0.084	Ala51, Ser122, Arg240	Gly50, Glu53, Tyr58, His121, Met123, Leu148, Ser155, Gly177, Pro178, Asp180, Val183, Leu184, Tyr194, Leu205, ***Cys242*, His269**, Val270	Leu241, Ile179, Ala51, Leu213
ZYH (MGL inhibitor)	0.000325	Ala51	Gly50, Gly52, Glu53, Arg57, **Ser122**, Met123, Leu148, Ala156, Phe159, Asp180, Ser181, Ser185, Asn187, Glu190, Leu205, Gly210, Leu214, Val217, **His269**, Lys273	Leu241, Tyr194, Leu184, Val191, Val270, Ile179, His121, Leu213, Ala151

Notes: Black bold indicates triad amino acid residue in the catalytic pocket of human MGL; ***Bold italics*** indicates important amino acid residue for inhibition of human MGL.

sitosterol and stigmasterol toward the enzyme, thus revealing the potential of these phytosterols in inhibiting MGL. The results of the molecular docking simulation are tabulated in Table 3.

The Dynamics Stability of the Ligand-MGL Complex (in Terms of RMSD and RMSF)

The dynamic stability of stigmasterol/MGL and beta-sitosterol/MGL within 250 ns is determined using MD simulation, and compared to that of ZYH/MGL and JZL195/MGL. The resulting RMSD and RMSF graphs are depicted in Figure 3.

Both complexes of stigmasterol/MGL (the yellow graph in Figure 3a) and beta-sitosterol/MGL (the grey graph in Figure 3a) exhibit a similar RMSD pattern to that of ZYH/MGL (the blue graph in Figure 3a), with an RMSD value of < 0.25 Å, thus confirming the stability of these complexes from their initial to final conformation. As described previously by Oubahmane et al, a stable protein will show minimal deviation in its backbone during the simulation.[24] Conversely, it is observed that the JZL195/MGL complex (the dark orange graph in Figure 3a) is not stable at 50–70 ns of simulation with an RMSD value of 0.32 Å and at 240 ns with an RMSD value of 0.28 Å. Respectively in a sequential manner, the average RMSD value of the ZYH/MGL complex, beta-sitosterol/MGL complex, stigmasterol/MGL complex, and JZL195/MGL complex was 0.172 Å, 0.192 Å, 0.200 Å, and 0.211 Å, which further confirms the best stability of the beta-sitosterol/MGL complex.

Meanwhile, in Figure 3b the RMSF pattern of ZYH/MGL, JZL195/MGL, beta-sitosterol/MGL, and stigmasterol/MGL within 250 ns simulation resulted in similar flexible regions on residues 150 to 180, located at the lid domain of the

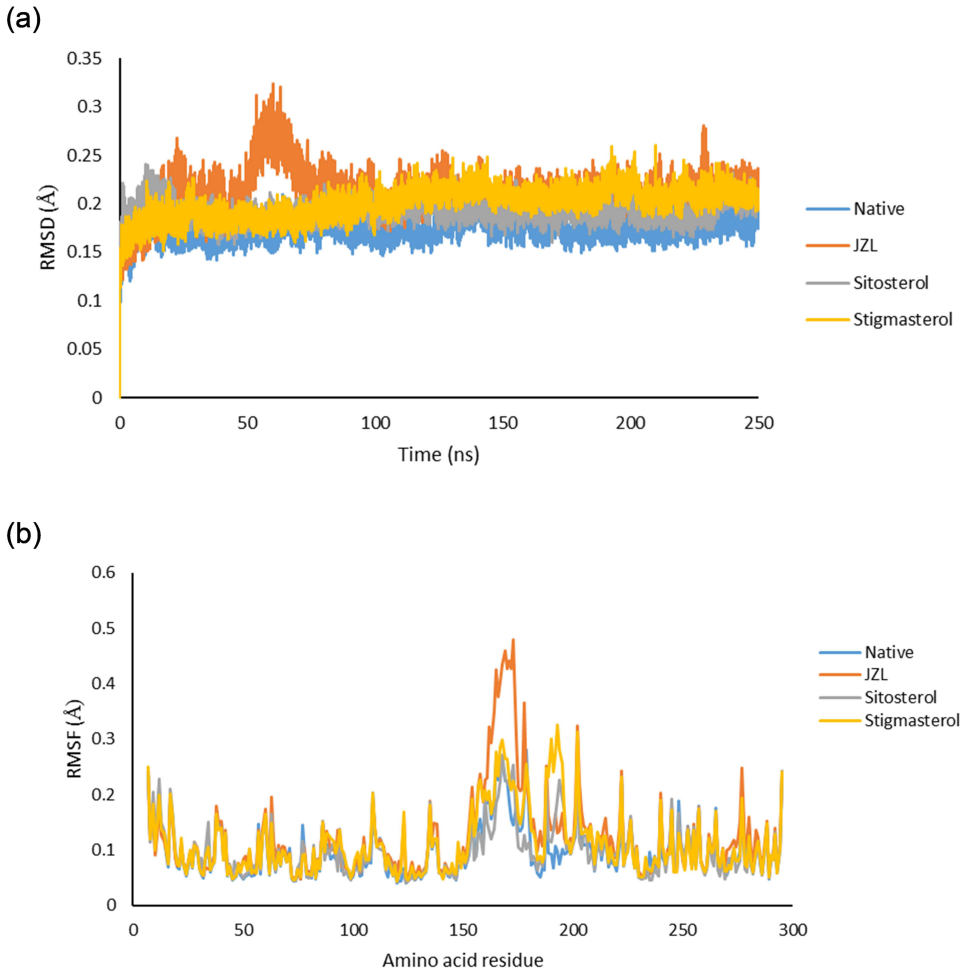

Figure 3 The RMSD (**a**) and RMSF (**b**) graphs of ZYH (blue), JZL195 (dark Orange), beta-sitosterol (grey), and stigmasterol (yellow) in complex with MGL within 250 ns MD simulation.

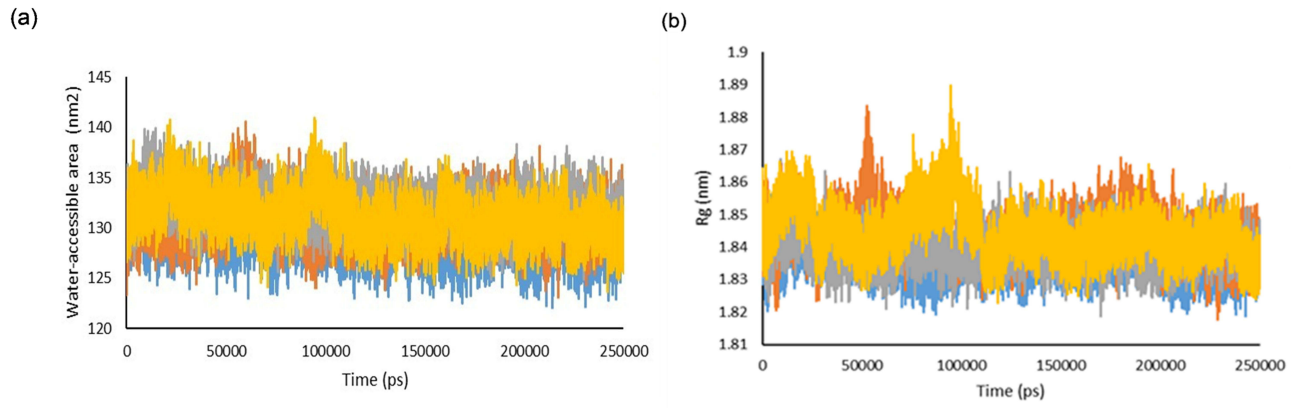

Figure 4 The (**a**) solvent accessible surface area (SASA) and (**b**) radius of gyration (Rg) plot of ZYH/MGL (blue), JZL195/MGL (Orange), beta-sitosterol/MGL (grey), and stigmasterol/MGL (yellow) within 250 ns MD simulation.

enzyme. However, residues 165, 169,173, and 178 in JZL195 revealed a higher fluctuative pattern (RMSF value reaches 0.49 Å at residue 178) than the other complexes, thus indicating the instability of the JZL/MGL complex. It is defined that RMSF is used to identify the flexible regions of the protein-ligand complexes and less-stable proteins will show higher RMSF fluctuations.[24] It was described in a recent article that as a highly dynamic structure, the lid domain of human MGL, comprised of amino acid residues 151–225, acts as a portal and contributes a pivotal role in the enzyme function by managing the access of 2-AG (the substrate) to the catalytic pocket. In particular, residue Asp239 is considered important for the conformational gating of the enzyme. Residues at the portal and the residues at the catalytic pocket may be appropriate for both open- and closed-type configurations. Two backbone amide groups of Leu241 and Cys242 function as anchor groups to stabilize the catalytic acid.[41]

Trajectory Analysis and Visualization (MM-PBSA Binding Free Energy Calculations)

The resulting SASA analysis and Rg graphs are depicted in Figure 4. In this study, SASA was analyzed during 250 ns of MD trajectory simulation. The SASA values (Figure 4a) are, respectively, ZYH/MGL 126.777 nm^2, JZL195/MGL 130.445 nm^2, beta-sitosterol/MGL 131.733 nm^2, and stigmasterol/MGL 130.373 nm^2, revealing similar values and patterns between all complexes, thus further confirming that beta-sitosterol and stigmasterol may work as potential inhibitors of human MGL. Interestingly, the stigmasterol/MGL complex shows better stability than beta-sitosterol/MGL.

Protein solvent accessible surface area (SASA) is the region around a protein by the Van der Waals contact surface of the molecule and a hypothetical center of a solvent sphere. The changes in SASA quantities illustrate the folding and unfolding of complexes. A lower SASA value indicates greater compactness.[42] A larger value of the protein SASA during simulation may also indicate structural relaxation and reduced protein stability.[43,44]

The next parameter is the radius of gyration (Rg), a rudimentary indicator to measure the stability of a protein structure during MD simulations. The Rg analyzes the compactness manner and flexibility of the protein inside a biological environment. The lower values of Rg describe a more rigid structure during the simulation.[45] Meanwhile, the average Rg values (Figure 4b) are, respectively, ZYH/MGL 1.836 nm, beta-sitosterol/MGL 1.839 nm, JZL195/MGL

Table 4 MM-PBSA Binding Free Energy Calculations

Protein name	Ligand	Van der Waals Energy (kJ/mol)	Electrostatic Energy (kJ/mol)	Polar Solvation Energy (kJ/mol)	SASA Energy (kJ/mol)	Total Binding Energy (kJ/mol)
MGL	ZYH	−293.51 ± 12.74	−48.30 ± 8.79	191.06 ± 12.76	−25.06 ± 0.78	−175.81 ± 17.14
	JZL195	−253.22 ± 14.26	−10.57 ± 6.56	141.85 ± 19.37	−24.25 ± 0.86	−146.19 ± 18.31
	Beta-sitosterol	−253.04 ± 13.52	−11.54 ± 9.93	98.68 ± 10.88	−25.05 ± 0.79	−190.95 ± 14.73
	Stigmasterol	−241.10 ± 18.24	−15.60 ± 7.51	93.14 ± 19.02	−24.35 ± 0.77	−187.91 ± 28.11

1.844 nm, and the stigmasterol/MGL 1.844 nm, revealing similar values and patterns between all complexes. The beta-sitosterol/MGL complex shows a more rigid structure than that of stigmasterol/MGL.

The MM-PBSA binding free energy calculations within 0–250 ns are presented in Table 4. This step resulted in negative values for the Van der Waals, electrostatic, and SASA energies in both complex systems, while the polar solvation energy was positive. The binding free energy of beta-sitosterol (−190.949 kJ/mol) and stigmasterol (−187.907 kJ/mol) is lower than ZYH (−175.810 kJ/mol) and JZL195 (−146.190 kJ/mol), thus indicating that both phytosterols have a stronger affinity for the MGL receptor.

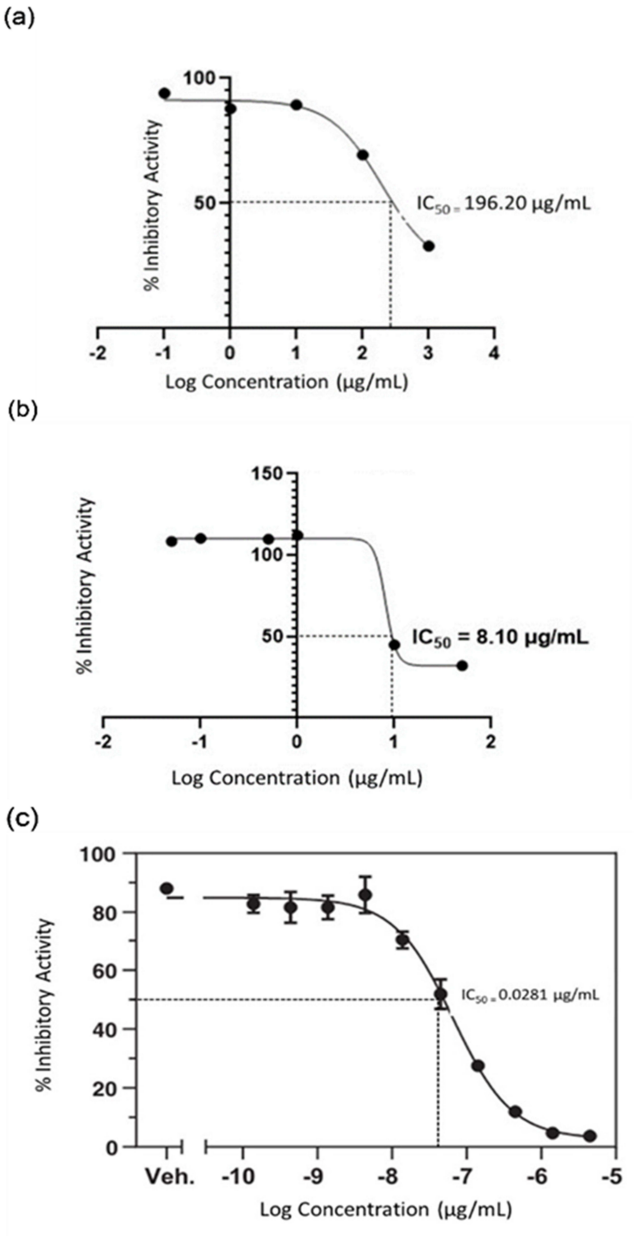

Figure 5 The human monoacylglycerol lipase (MGL) inhibitory activity graph of (**a**) *M. citrifolia* fruit extract (EEMC) with an IC_{50} value of 196.20 ± 25.169 µg/mL; (**b**) beta-sitosterol with an IC_{50} value of 8.10 ± 37.255 µg/mL; and (**c**) JZL195 with an IC_{50} value of 0.0281 ± 51.662 µg/mL. The measurement was replicated 3x. Data are presented as mean ± SD.

Effects of EEMC on Human Monoacylglycerol Lipase by in vitro Study

In our study, beta-sitosterol and EEMC could inhibit human MGL, with an IC_{50} value of 8.10 8.10 ± 37.255 µg/mL and 196.20 ± 25.169 µg/mL, respectively. At the same time, JZL195, a known inhibitor of the enzyme, showed an IC_{50} value of 0.0281 ± 51.662 µg/mL (Figure 5). The measurement was replicated 3x. Data are presented as mean ± SD.

Discussion

The catalytic site of human MGL is characterized by the triad residues Ser122, Asp239, and His269.[3] These triad residues are located at the rear end of the long passage under the lid domain of the enzyme.[41] To inhibit the enzyme, it is suggested that the inhibitors build a covalent interaction with Cys208 and Cys242 in the catalytic site.[3,4,46] Because of the important roles of MGL in the regulation of endocannabinoid and eicosanoid signaling pathways, the wide hydrophobic entry to the catalytic site of MGL, with the entry edge nearby hydrophobic helixes, allows MGL to interact with membranes and recruit lipophilic substrates. The three cysteine residues (Cys201, Cys208, and Cys242) located near the catalytic triad were described to function together in stabilizing the active conformation of MGL. These residues have been reported to be the target of isothiazolinone-based MGL inhibitors.[46]

Our molecular docking simulation discloses that both phytosterols (stigmasterol and beta-sitosterol) and MGL inhibitors (co-crystallized inhibitor ZYH and JZL195) could enter and occupy the catalytic site of the enzyme and bind with essential amino acid residues with considerable affinity. Of those, only beta-sitosterol and JZL195 interact with Cys242, one of the important residues required to inhibit MGL activity,[3,4] thus revealing their potential to inhibit human MGL, and may play a role in neuroprotective activity against inflammatory damage. Indeed, we confirm that the four compounds possess the required three features for MGL inhibitors as described by Afzal et al. The pharmacophore features for MGL inhibitors are one hydrogen bond acceptor (HBA), one positive center, and three aromatic rings.[5]

In our study, the in silico pharmacology was continued by performing the in vitro protocol of the extract (EEMC) and standard beta-sitosterol towards the human MGL enzyme. Combining in silico and in vitro techniques has been widely reported to guarantee the validity of the results.[47–49] A previous work of Jusril et al in 2020 reported in silico and in vitro studies to evaluate the acetylcholinesterase inhibitory profile of triterpenes of *Centella asiatica*.[47] Another study which was recently published in 2023 combined in silico and in vitro studies to understand the structural insights and nucleotide-binding ability of the transcriptional regulator PehR from *Ralstonia solanacearum*.[48] Moreover, Zhu and coworkers reported the molecular mechanisms of natural stable angiotensin-converting enzyme inhibitory peptides from foxtail millet protein hydrolysates by combining in silico and in vitro studies, published in 2024.[49]

Phytosterols have been broadly explored for their activity in maintaining neuron homeostasis in the body due to their ability to penetrate the blood-brain barrier. Stigmasterol isolated from *Artemisia indica* could increase GABA-induced currents at the ternary α2β2γ2L, α4β3δ, and binary α4β3 subtypes of the $GABA_A$ receptor.[50] Neuron cells pre-incubated with stigmasterol showed an increase of catalase and Bcl-2, suggesting its neuroprotective effect.[51] Stigmasterol treatment reduced the expression of N-methyl-D-acetate receptor subunit 2B (GluN2B) and vesicular glutamate transporter 1 (VGLUT1).[52] Stigmasterol could alleviate neurodegeneration induced by oxidative stress.[53] A previous study reported that beta-sitosterol treatment in double transgenic mice expressing a chimeric mouse/human amyloid precursor protein (APP/PS1) could improve spatial learning and recognition memory ability.[54]

Inhibition of MGL has unlocked promising neuroprotective effects in various preclinical models, including those of neurodegenerative diseases, however, the specific impact of MGL inhibition on ischemic stroke is still an ongoing research. The inhibition of MGL may confer neuroprotection against ischemic injury by modulating endocannabinoid signaling, reducing excitotoxicity, oxidative stress, and inflammation.[55,56] Ischemic stroke could trigger excitotoxicity, primarily mediated by excessive glutamate release and subsequent neuronal hyperexcitation. MGL inhibition and subsequent elevation of 2-AG levels may attenuate excitotoxicity and protect neurons from glutamate-induced damage.[57] Ischemic stroke-induced inflammation exacerbates tissue damage and contributes to secondary injury. Interestingly, MGL inhibition has been shown to reduce neuroinflammation by modulating immune cell activation and cytokine production, thereby limiting inflammatory damage in the ischemic brain,[58] and enhancing cerebral blood flow,

thus improving perfusion to ischemic regions of the brain.[59] Studies in other neurological conditions have demonstrated improved neurological outcomes, reduced infarct volume, and enhanced neuronal survival upon MGL inhibition.[60]

JZL195 is a known MGL inhibitor with a non-selective inhibition or dual inhibitory mechanism to both MGL and FAAH (fatty acid amide hydrolase). JZL195 was developed by Long et al in 2009,[61] and recently this inhibitor was reported to induce a significant enhancement of 2-AG levels in rats' brains.[62] In our study, JZL195 strongly inhibits MGL activity with an IC_{50} of 0.0281 µg/mL, meanwhile, beta-sitosterol and EEMC have the potential to inhibit MGL activity with an IC_{50} value of, respectively, 8.10 and 196.20 µg/mL.

Conclusion

Morinda citrifolia fruits contain phytosterols with hydrophobic properties and thus can penetrate the blood-brain barrier. Phytosterols are interesting to study because they possess pharmacophoric features required for occupying the catalytic site of human MGL. In this study, beta-sitosterol and stigmasterol have the potential to inhibit the enzyme, however, beta-sitosterol shows a better stability complex with human MGL than stigmasterol. Its inhibitory activity is comparable to that of JZL195, as evidenced by binding modes, RMSD, RMSF, Rg, SASA, and MM-PBSA calculations. Moreover, beta-sitosterol and the ethanol extract of *M. citrifolia* fruit can inhibit human MGL with an IC_{50} value of, respectively, 8.10 and 196.20 µg/mL. Considering this, *M. citrifolia* fruit may combat inflammatory damage in the neurons by inhibiting MGL, whose activity is contributed by the phytosterols.

Acknowledgments

The authors thank the Rector of Universitas Padjadjaran University for funding both the research (via the Universitas Padjadjaran Academic-Leadership Grant 2024) and the APC (via the Directorate of Research and Community Engagement). This work is in the framework of the doctoral research of the first author at the Doctoral Program in Pharmacy, Faculty of Pharmacy, Universitas Padjadjaran, West Java, Indonesia.

Funding

This work is funded by the Universitas Padjadjaran Academic-Leadership Grant 2024 document contract No. 1479/UN6.3.1/PT.00/2024 of Prof. Dr. Jutti Levita.

Disclosure

The authors declare no conflicts of interest.

References

1. Wei D, Lee D, Li D, Daglian J, Jung KM, Piomelli D. A role for the endocannabinoid 2-arachidonoyl-sn-glycerol for social and high-fat food reward in male mice. *Psychopharmacology*. 2016;233(10):1911–1919. doi:10.1007/2Fs00213-016-4222-0
2. Dinh TP, Freund TF, Piomelli D. A role for monoglyceride lipase in 2-arachidonoylglycerol inactivation. *Chem Phys Lipids*. 2002;121(1–2):149–-158. doi:10.1016/s0009-3084(02)00150-0
3. Zvonok N, Pandarinathan L, Williams J, et al. Covalent inhibitors of human monoacylglycerol lipase: ligand-assisted characterization of the catalytic site by mass spectrometry and mutational analysis. *Chem Biol*. 2008;15(8):854–862. doi:10.1016/j.chembiol.2008.06.008
4. Labar G, Bauvois C, Muccioli GG, Wouters J, Lambert DM. Disulfiram is an inhibitor of human-purified monoacylglycerol lipase, the enzyme regulating 2-arachidonoylglycerol signaling. *Chembiochem*. 2007;8(11):1293–1297. doi:10.1002/cbic.200700139
5. Afzal O, Kumar S, Kumar R, Firoz A, Jaggi M, Bawa S. Docking-based virtual screening and molecular dynamics study to identify potential monoacylglycerol lipase inhibitors. *Bioorg Med Chem Lett*. 2014;24(16):3986–3996. doi:10.1016/j.bmcl.2014.06.029
6. Jha V, Biagi M, Spinelli V, et al. Discovery of monoacylglycerol lipase (MAGL) inhibitors based on a pharmacophore-guided virtual screening study. *Molecules*. 2020;26(1):78. doi:10.3390/molecules26010078
7. Grabner GF, Zimmermann R, Schicho R, Taschler U. Monoglyceride lipase as a drug target: at the crossroads of arachidonic acid metabolism and endocannabinoid signaling. *Pharmacol Ther*. 2017;175:35–46. doi:10.1016/j.pharmthera.2017.02.033
8. Marsicano G, Goodenough S, Monory K, et al. CB1 cannabinoid receptors and on-demand defense against excitotoxicity. *Science*. 2003;302(5642):84–88. doi:10.1126/science.1088208
9. Panikashvili D, Simeonidou C, Ben-Shabat S, et al. An endogenous cannabinoid (2-AG) is neuroprotective after brain injury. *Nature*. 2001;413(6855):527–531. doi:10.1038/35097089
10. Zanfirescu A, Ungurianu A, Mihai DP, Radulescu D, Nitulescu GM. Targeting monoacylglycerol lipase in pursuit of therapies for neurological and neurodegenerative diseases. *Molecules*. 2021;26(18):5668. doi:10.3390/molecules26185668

11. Walter L, Franklin A, Witting A, et al. Nonpsychotropic cannabinoid receptors regulate microglial cell migration. *J Neurosci*. 2003;23(4):1398–1405. doi:10.1523/jneurosci.23-04-01398.2003
12. Gauci AJ, Caruana M, Giese A, Scerri C, Vassallo N. Identification of polyphenolic compounds and black tea extract as potent inhibitors of lipid membrane destabilization by Aβ aggregates. *J Alzheimers Dis*. 2011;27(4):767–779. doi:10.3233/jad-2011-111061
13. Wu CR, Lin HC, Su MH. Reversal by aqueous extracts of Cistanche tubulosa from behavioral deficits in Alzheimer's disease-like rat model: relevance for amyloid deposition and central neurotransmitter function. *BMC Complement Altern Med*. 2014;14:202. doi:10.1186/2F1472-6882-14-202
14. Polito CA, Cai ZY, Shi YL, et al. Association of tea consumption with risk of Alzheimer's disease and anti-beta-amyloid effects of tea. *Nutrients*. 2018;10(5):655. doi:10.3390/nu10050655
15. Firdaus Z, Singh N, Prajapati SK, Krishnamurthy S, Singh TD. *Centella asiatica* prevents D-galactose-Induced cognitive deficits, oxidative stress and neurodegeneration in the adult rat brain. *Drug Chem Toxicol*. 2022;45(3):1417–1426. doi:10.1080/01480545.2020.1833907
16. Ali M, Singh P, Singh L, Pandey RK, Soni P, Singh A. Neuroprotective effect of Morinda citrifolia on behavioural and biochemical deficits in PTZ-induced kindled mice. *Infect Disord Drug Targets*. 2023;23(8):30–42. doi:10.2174/1871526523666230605160222
17. King AR, Dotsey EY, Lodola A, et al. Discovery of potent and reversible monoacylglycerol lipase inhibitors. *Chem Biol*. 2009;16(10):1045–1052. doi:10.1016/j.chembiol.2009.09.012
18. Tosco P, Stiefl N, Landrum G. Bringing the MMFF force field to the RDKit: implementation and validation. *J Cheminform*. 2014;6(1):4–7. doi:10.1186/s13321-014-0037-3
19. Lolok N, Sumiwi SA, Muhtadi A, et al. Molecular docking and molecular dynamics studies of bioactive compounds contained in noni fruit (Morinda citrifolia L.) against human pancreatic α-amylase. *J Biomol Struct Dyn*. 2022;40(15):7091–7098. doi:10.1080/07391102.2021.1894981
20. Aulifa DL, Adnyana IK, Levita J, Sukrasno S. 4-Hydroxyderricin isolated from the sap of Angelica keiskei Koidzumi: evaluation of its inhibitory activity towards dipeptidyl peptidase-IV. *Sci Pharm*. 2019;87(4):30. doi:10.3390/scipharm87040030
21. Mutakin, Saptarini NM, Amalia R, et al. Molecular docking simulation of phenolics towards tyrosinase, phenolic content, and radical scavenging activity of some Zingiberaceae plant extracts. *Cosmetics*. 2023;10(6):149. doi:10.3390/cosmetics10060149
22. Aulifa DL, Amirah SR, Rahayu D, Megantara S, Muchtaridi M. Pharmacophore modeling and binding affinity of secondary metabolites from Angelica keiskei to HMG co-A reductase. *Molecules*. 2024;29(13):2983. doi:10.3390/molecules29132983
23. Abraham MJ, Murtola T, Schulz R, et al. Gromacs: high-performance molecular simulations through multi-level parallelism from laptops to supercomputers. *SoftwareX*. 2015;1–2:19–25. doi:10.1016/j.softx.2015.06.001
24. Oubahmane M, Hdoufane I, Delaite C, Sayede A, Cherqaoui D, El Allali A. Design of potent inhibitors targeting the main protease of SARS-CoV-2 using QSAR modeling, molecular docking, and molecular dynamics simulations. *Pharmaceuticals*. 2023;16(4):608. doi:10.3390/ph16040608
25. Zhang ZW, Lu WC. AmberMDrun: a scripting tool for running Amber MD in an easy way. *Biomolecules*. 2023;13(4):635. doi:10.3390/biom13040635
26. Weng YL, Naik SR, Dingelstad N, Lugo MR, Kalyaanamoorthy S, Ganesan A. Molecular dynamics and in silico mutagenesis on the reversible inhibitor-bound SARS-CoV-2 main protease complexes reveal the role of lateral pocket in enhancing the ligand affinity. *Sci Rep*. 2021;11(1):1–22. doi:10.1038/s41598-021-86471-0
27. Zeyaullah M, Khan N, Muzammil K, et al. In-silico approaches for identification of compounds inhibiting SARS-CoV-2 3CL protease. *PLoS One*. 2023;18(4):1–27. doi:10.1371/journal.pone.0284301
28. Essmann U, Perera L, Berkowitz ML, Darden T, Lee H, Pedersen LG. A smooth particle mesh Ewald method. *J Chem Phys*. 1995;103(19):8577–8593. doi:10.1063/1.470117
29. Elftmaoui Z, Bignon E. Robust AMBER Force Field Parameters for glutathionylated cysteines. *Int J Mol Sci*. 2023;24(19):15022. doi:10.3390/ijms241915022
30. Mark P, Nilsson L. Structure and dynamics of the TIP3P, SPC, and SPC/E water models at 298 K. *J Phys Chem A*. 2001;105(43):9954–9960. doi:10.1021/jp003020w
31. Kubitzki MB, De Groot BL. Molecular dynamics simulations using temperature-enhanced essential dynamics replica exchange. *Biophys J*. 2007;92(12):4262–4270. doi:10.1529/biophysj.106.103101
32. Wang C, Greene D, Xiao L, Qi R, Luo R. Recent developments and applications of the MMPBSA method. *Front Mol Biosci*. 2018;4:1–18. doi:10.3389/fmolb.2017.00087
33. Truchon JF, Nicholls A, Roux B, Iftimie RI, Bayly CI. Integrated continuum dielectric approaches to treat molecular polarizability and the condensed phase: refractive index and implicit solvation. *J Chem Theory Comput*. 2009;5(7):1785–1802. doi:10.1021/ct900029d
34. Alanzi AR, Parvez MK, Al-Dosari MS. Structure-based virtual identification of natural inhibitors of SARS-CoV-2 and its Delta and Omicron variant proteins. *Future Virol*. 2023;18(7):421–438. doi:10.2217/fvl-2022-0184
35. Backer CA, Bakhuizen Van Den Brink RC Flora of Java (Spermatophytes only). Vol. 2; 1965.
36. Kesonbuaa W, Chantaranothai P, Naqvi SA, et al. The genus Morinda (Rubiaceae) in Thailand. *Sci Asia*. 2013;39(3):331–339. doi:10.2306/scienceasia1513-1874.2013.39.331
37. Das SC, Rahman MA. Taxonomic revision of the genus Morinda L.(Rubiaceae) in Bangladesh. *Bangladesh J Bot*. 2011;40(2):113–120. doi:10.3329/bjb.v40i2.9766
38. World Health Organization. *Quality Control Methods for Medicinal Plant Materials*. World Health Organization; 1998.
39. Muccioli GG, Labar G, Lambert DM. CAY10499, a novel monoglyceride lipase inhibitor evidenced by an expeditious MGL assay. *Chembiochem*. 2008;9(16):2704–2710. doi:10.1002/cbic.200800428
40. Zvonok N, Williams J, Johnston M, et al. Full mass spectrometric characterization of human monoacylglycerol lipase generated by large-scale expression and single-step purification. *J Proteome Res*. 2008;7(5):2158–2164. doi:10.1021/pr700839z
41. Tyukhtenko S, Ma X, Rajarshi G, et al. Conformational gating, dynamics and allostery in human monoacylglycerol lipase. *Sci Rep*. 2020;10(1):1–16. doi:10.1038/s41598-020-75497-5
42. Ali S, Hassan M, Islam A, Ahmad F. A review of methods available to estimate solvent-accessible surface areas of soluble proteins in the folded and Unfolded States. *Curr Protein Pept Sci*. 2014;15(5):456–476. doi:10.2174/1389203715666140327114232
43. Mattea C, Qvist J, Halle B. Dynamics at the protein-water interface from 17O spin relaxation in deeply supercooled solutions. *Biophys J*. 2008;95(6):2951–2963. doi:10.1529/biophysj.108.135194

44. Damjanovic A, Brooks BR, Garcia-Moreno B. Conformational relaxation and water penetration coupled to ionization of internal groups in proteins. *J Phys Chem*. 2011;115:4042–4053. doi:10.1021/jp110373f
45. Ghahremanian S, Rashidi MM, Raeisi K, Toghraie D. Molecular dynamics simulation approach for discovering potential inhibitors against SARS-CoV-2: a structural review. *J Mol Liq*. 2022;354:118901. doi:10.1016/j.molliq.2022.118901
46. King AR, Lodola A, Carmi C, Fu J, Mor M, Piomelli D. A critical cysteine residue in monoacylglycerol lipase is targeted by a new class of isothiazolinone-based enzyme inhibitors. *Br J Pharmacol*. 2009;157(6):974–983. doi:10.1111/j.1476-5381.2009.00276.x
47. Jusril NA, Muhamad Juhari ANN, Abu Bakar SI, Md Saad WM, Adenan MI. Combining In silico and in vitro studies to evaluate the acetylcholinesterase inhibitory profile of different accessions and the biomarker triterpenes of *Centella asiatica*. *Molecules*. 2020;25(15):3353. doi:10.3390/molecules25153353
48. Yadav M, Sarkar S, Olymon K, Ray SK, Kumar A. Combined in silico and in vitro study to reveal the structural insights and nucleotide-binding ability of the transcriptional regulator pehr from the phytopathogen *Ralstonia solanacearum*. *ACS Omega*. 2023;8(38):34499–34515. doi:10.1021/acsomega.3c03175
49. Zhu Y, Chen C, Dai Z, et al. Identification, screening and molecular mechanisms of natural stable angiotensin-converting enzyme (ACE) inhibitory peptides from foxtail millet protein hydrolysates: a combined in silico and in vitro study. *Food Funct*. 2024;15(15):7782–7793. doi:10.1039/d4fo01992j
50. Karim N, Khan I, Abdelhalim A, Halim SA, Khan A, Al-Harrasi A. Stigmasterol can be new steroidal drug for neurological disorders: evidence of the GABAergic mechanism via receptor modulation. *Phytomedicine*. 2021;90:153646. doi:10.1016/j.phymed.2021.153646
51. Lee J, Weon JB, Ma CJ. Neuroprotective activity of phytosterols isolated from Artemisia apiacea. *Korean J Pharmacogn*. 2014;45(3):214–219.
52. Haque MN, Hannan MA, Dash R, Choi SM, Moon IS. The potential LXRβ agonist stigmasterol protects against hypoxia/reoxygenation injury by modulating mitophagy in primary hippocampal neurons. *Phytomedicine*. 2021;81:153415. doi:10.1016/j.phymed.2020.153415
53. Pratiwi R, Nantasenamat C, Ruankham W, et al. Mechanisms and neuroprotective activities of stigmasterol against oxidative stress-induced neuronal cell death via Sirtuin family. *Front Nutr*. 2021;8:1–12. doi:10.3389/fnut.2021.648995
54. Ye JY, Li L, Hao QM, Qin Y, Ma CS. β-Sitosterol treatment attenuates cognitive deficits and prevents amyloid plaque deposition in amyloid protein precursor/presenilin 1 mice. *Korean J Physiol Pharmacol*. 2020;24(1):39–46. doi:10.4196/kjpp.2020.24.1.39
55. Hill MN, McLaughlin RJ, Pan B, et al. Recruitment of prefrontal cortical endocannabinoid signaling by glucocorticoids contributes to termination of the stress response. *J Neurosci*. 2011;31(29):10506–10515. doi:10.1523/JNEUROSCI.0496-11.2011
56. Zhang J, Teng Z, Song Y, Hu M, Chen C. Inhibition of monoacylglycerol lipase prevents chronic traumatic encephalopathy-like neuropathology in a mouse model of repetitive mild closed head injury. *J Perinatol*. 2015;35(3):443–453. doi:10.1038/jcbfm.2014.216
57. Nomura DK, Morrison BE, Blankman JL, et al. Endocannabinoid hydrolysis generates brain prostaglandins that promote neuroinflammation. *Science*. 2011;334(6057):809–813. doi:10.1126/science.1209200
58. Piro JR, Benjamin DI, Duerr JM, et al. A Dysregulated endocannabinoid-eicosanoid network supports pathogenesis in a mouse model of Alzheimer's disease. *Cell Rep*. 2012;1(6):617–623. doi:10.1016/j.celrep.2012.05.001
59. Nomura DK, Hudak CSS, Ward AM, et al. Monoacylglycerol lipase regulates 2-arachidonoylglycerol action and arachidonic acid levels. *Bioorganic Med Chem Lett*. 2008;18(22):5875–5878. doi:10.1016/j.bmcl.2008.08.007
60. Mulvihill MM, Nomura DK. Therapeutic potential of monoacylglycerol lipase inhibitors. *Life Sci*. 2013;92(8–9):492–497. doi:10.1016/j.lfs.2012.10.025
61. Long JZ, Nomura DK, Vann RE, et al. Dual blockade of FAAH and MAGL identifies behavioral processes regulated by endocannabinoid crosstalk in vivo. *Proc Natl Acad Sci USA*. 2009c;106:20270–20275. doi:10.1073/pnas.0909411106
62. Seillier A, Dominguez Aguilar D, Giuffrida A. The dual FAAH/MAGL inhibitor JZL195 has enhanced effects on endocannabinoid transmission and motor behavior in rats as compared to those of the MAGL inhibitor JZL184. *Pharmacol Biochem Behav*. 2014;124:153–159. doi:10.1016/j.pbb.2014.05.022